

Signal Correlation Modeling in Acoustic Vector Sensor Arrays

A. Abdi*, *Senior Member, IEEE*, and H. Guo, *Student Member, IEEE*

Abstract – A vector sensor measures the scalar and vector components of the acoustic field. In a multipath channel, the sensor collects the information via multiple paths. Depending on the angle of arrival distribution and other channel characteristics, different types of correlation appear in a vector sensor array, which affect the array performance. In this paper a novel statistical framework is developed which provides closed-form parametric expressions for signal correlations in vector sensor arrays. Such correlation expressions serve as useful tools for system design and performance analysis of vector sensor signal processing algorithms. They can also be used to estimate some important physical parameters of the channel such as angle spreads, mean angle of arrivals, etc.

EDICS: SSP-SNMD (Statistical Signal Processing-Signal and Noise Modeling)

Copyright (c) 2008 IEEE. Personal use of this material is permitted.

However, permission to use this material for any other purposes must be obtained from the IEEE by sending a request to pubs-permissions@ieee.org.

A. Abdi (**corresponding author**) and H. Guo are with the Center for Wireless Communications and Signal Processing Research, Department of Electrical and Computer Engineering, New Jersey Institute of Technology, Newark, NJ 07102, USA.

Email: abdi@adm.njit.edu

Phone: 973-596-5621

Fax: 973-596-5680

1. INTRODUCTION

A vector sensor measures important non-scalar components of the acoustic field such as particle velocity and acceleration, which cannot be measured by a single scalar pressure sensor [1]. They have been used for SONAR and target localization [1]-[8], to accurately estimate the azimuth and elevation of a source [1] [7], to avoid the left-right ambiguity in linear towed arrays of scalar sensors, and to reduce acoustic noise due to their directive beam pattern [8]. Application of vector sensors as multichannel underwater equalizers is recently studied [9] [10].

In general, there are two types of vector sensors: inertial and gradient. Inertial sensors truly measure the velocity or acceleration by responding to the acoustic particle motion, whereas gradient sensors employ a finite-difference approximation to estimate the gradients of the acoustic field such as velocity and acceleration. Each sensor type has its own merits and limitations [11]. Depending on the application, system cost, required precision, etc., one can choose the proper sensor type and technology.

In multipath channels, a vector sensor receives the signal through multiple paths. This introduces different levels of correlation in an array of vector sensors. Characterization of these correlations in terms of the physical parameters of the channel are needed for proper system design, to achieve the required performance in the presence of correlations [12]-[14]. Furthermore, closed-form parametric expressions for the signal correlations serve as useful tools to estimate some important physical parameters of the channel such as angle spread, mean angle of arrival, etc. [15]-[17].

In what follows, basic formulas and definitions for signals in a vector sensor array are provided in Section 2. Then statistical models for pressure and velocity channels are developed in Section 3. General correlation functions for a vector sensor array are derived in Section 4, assuming an arbitrary angle of arrival distribution. For a Gaussian angle of arrival distribution, closed-form expressions are derived in Section 5 for various correlation functions of interest in vector sensor arrays. Comparison with experimental data is carried out in Section 6 and concluding remarks are provided in Section 7.

2. BASIC DEFINITIONS IN A VECTOR SENSOR ARRAY

Consider a vector sensor system implemented in a shallow water channel, as shown in Fig. 1. In the two-dimensional y - z (range-depth) plane, there is one pressure transmitter at the far field, called Tx and shown by a black dot. We also have two receive vector sensors, represented by two black squares, at $y = 0$ and the depths $z = z_1$ and $z_1 + L$, with L as the element spacing. The two receive sensors are called Rx_1 and Rx_2 , respectively. The array is located at the depth $z = D$, measured with respect to the center of the array. Each vector sensor measures the pressure, as well as the y and z components of the particle velocity, all in a single co-located point. This means that there are two pressure channels p_1 and p_2 , as well as four *pressure-equivalent* velocity channels p_1^y , p_1^z , p_2^y and p_2^z , all measured in Pascal (Newton/m²). In Fig. 1 the pressure channels are represented by straight dashed lines, whereas the pressure-equivalent velocity channels are shown by curved dashed lines. To define p_1^y , p_1^z , p_2^y and p_2^z , we need to define the velocity channels v_1^y , v_1^z , v_2^y and v_2^z , in m/s. According to the linearized momentum equation [18], the y and z components of the velocity at locations z_1 and $z_1 + L$ of the receive side and at the frequency f_0 can be written as

$$v_1^y = -\frac{1}{j\rho_0\omega_0} \frac{\partial p_1}{\partial y}, \quad v_1^z = -\frac{1}{j\rho_0\omega_0} \frac{\partial p_1}{\partial z}, \quad v_2^y = -\frac{1}{j\rho_0\omega_0} \frac{\partial p_2}{\partial y}, \quad v_2^z = -\frac{1}{j\rho_0\omega_0} \frac{\partial p_2}{\partial z}. \quad (1)$$

In the above equations, also known as the Euler's equation, ρ_0 is the density of the fluid in kg/m³, $j^2 = -1$, and $\omega_0 = 2\pi f_0$ is the frequency in rad/s. Eq. (1) simply states that the velocity in a certain direction is proportional to the spatial pressure gradient in that direction [18] [19]. To simplify the notation, similar to [18], we multiply the velocity channels in (1) with $-\rho_0 c$, the negative of the acoustic impedance of the fluid, where c is the speed of sound in m/s. This gives the associated *pressure-equivalent* velocity channels as $p_1^y = -\rho_0 c v_1^y$, $p_1^z = -\rho_0 c v_1^z$, $p_2^y = -\rho_0 c v_2^y$, and $p_2^z = -\rho_0 c v_2^z$. With λ as the wavelength in m and $k = 2\pi / \lambda = \omega_0 / c$ as the wavenumber in rad/m, we finally obtain

$$p_1^y = \frac{1}{jk} \frac{\partial p_1}{\partial y}, \quad p_1^z = \frac{1}{jk} \frac{\partial p_1}{\partial z}, \quad p_2^y = \frac{1}{jk} \frac{\partial p_2}{\partial y}, \quad p_2^z = \frac{1}{jk} \frac{\partial p_2}{\partial z}. \quad (2)$$

Each vector sensor in Fig. 1 provides three output signals. For example, Rx_1 generates one pressure signal r_1 and two pressure-equivalent velocity signals r_1^y and r_1^z , measured in the y and z directions, respectively. If s represent the transmitted signal, then the received signals can be written as

$$\begin{aligned} r_1 &= p_1 \oplus s + n_1, & r_2 &= p_2 \oplus s + n_2, \\ r_1^y &= p_1^y \oplus s + n_1^y, & r_2^y &= p_2^y \oplus s + n_2^y, \\ r_1^z &= p_1^z \oplus s + n_1^z, & r_2^z &= p_2^z \oplus s + n_2^z. \end{aligned} \quad (3)$$

In the above equation \oplus is convolution and each n stands for noise in a particular channel of a specific vector sensor. In the rest of the paper we concentrate on the characterization and analysis of the six channels p_1 , p_2 , p_1^y , p_1^z , p_2^y and p_2^z .

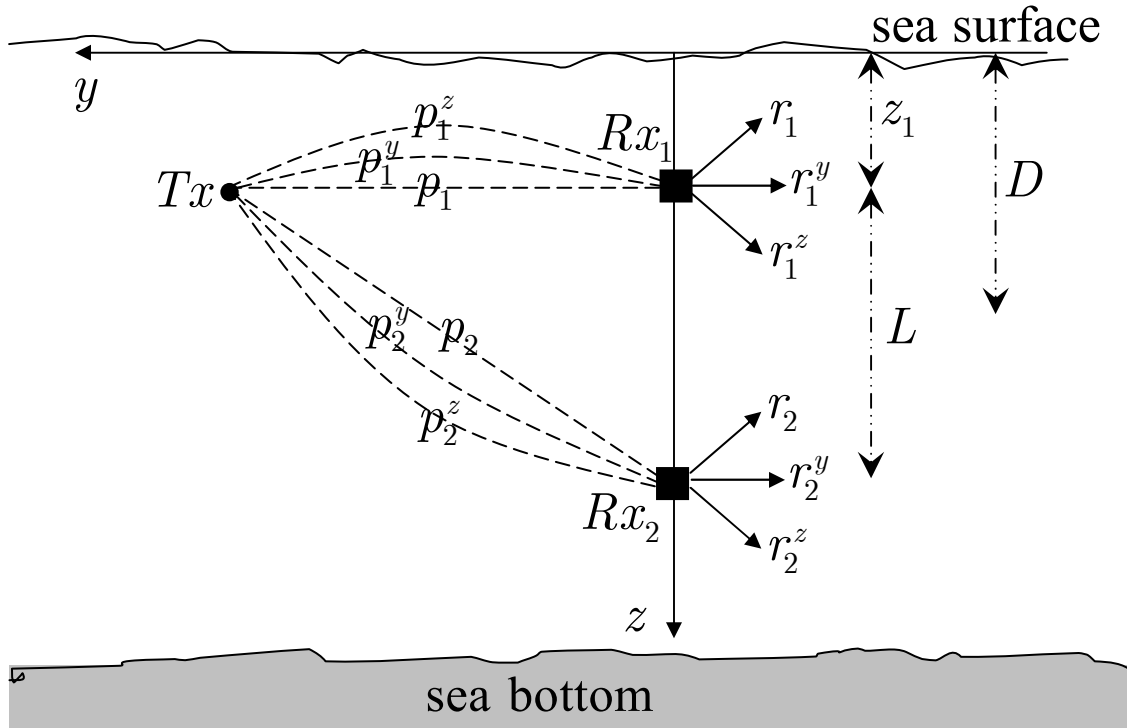


Fig. 1. A vector sensor system with one pressure transmitter and two vector sensor receivers. Each vector sensor measures the pressure, as well as the y and z component of the acoustic particle velocity, all in a single point.

3. STATISTICAL REPRESENTATION OF PRESSURE AND VELOCITY CHANNELS

An important multipath underwater channel is the shallow water acoustic channel. It is basically a waveguide, bounded from bottom and the top. The sea floor is a rough surface which

introduces scattering, reflection loss, and attenuation by sediments, whereas the sea surface is a rough surface that generates scattering and reflection loss and attenuation by turbidity and bubbles [20]. When compared with deep waters, shallow waters are more complex, due to the many interactions of acoustic waves with boundaries, which result in a significant amount of multipath propagation.

In this paper we develop a statistical framework, which concentrates on channel characterization using probabilistic models for the random components of the propagation environment. In this way, the statistical behavior of the channel can be imitated, and convenient closed-form expressions for the correlation functions of interest can be derived. These vector sensor parametric correlation expressions allow engineers to design, simulate, and assess a variety of design schemes under different channel conditions.

In what follows we provide proper statistical representations for pressure and velocity channels in shallow waters. These channel representations will be used in Section 4, to calculate different types of channel correlations.

3.1. Pressure-Related Channel Functions

In this subsection we define and focus on the three pressure channel functions $\chi(\gamma, \tau)$, $p(\tau)$ and $P(f)$, over the angle-delay, delay-space and frequency-space domains, respectively.

Fig. 2 shows the system of Fig. 1, as well as the geometrical details of the received rays in a shallow water channel, with two vector sensor receivers. Two-dimensional propagation of plane waves in the y - z (range-depth) plane is assumed, in a time-invariant environment with D_0 as the water depth. All the angles are measured with respect to the positive direction of y , counterclockwise. We model the rough sea bottom and its surface as collections of N^b and N^s scatterers, respectively, such that $N^b \gg 1$ and $N^s \gg 1$. In Fig. 2, the i -th bottom scatterer is represented by S_i^b , $i = 1, 2, \dots, N^b$, whereas S_m^s denotes the m -th surface scatterer, $m = 1, 2, \dots, N^s$. Rays scattered from the bottom and the surface are shown by solid thick and solid thin lines, respectively. The rays scattered from S_i^b hit Rx_1 and Rx_2 at the angle-of-arrivals (AOAs) $\gamma_{i,1}^b$ and $\gamma_{i,2}^b$, respectively. The traveled distances are labeled by $\xi_{i,1}^b$ and $\xi_{i,2}^b$, respectively. Similarly,

the scattered rays from S_m^s impinge Rx_1 and Rx_2 at the AOAs $\gamma_{m,1}^s$ and $\gamma_{m,2}^s$, respectively, with $\xi_{m,1}^s$ and $\xi_{m,2}^s$ as the traveled distances shown in Fig. 2.

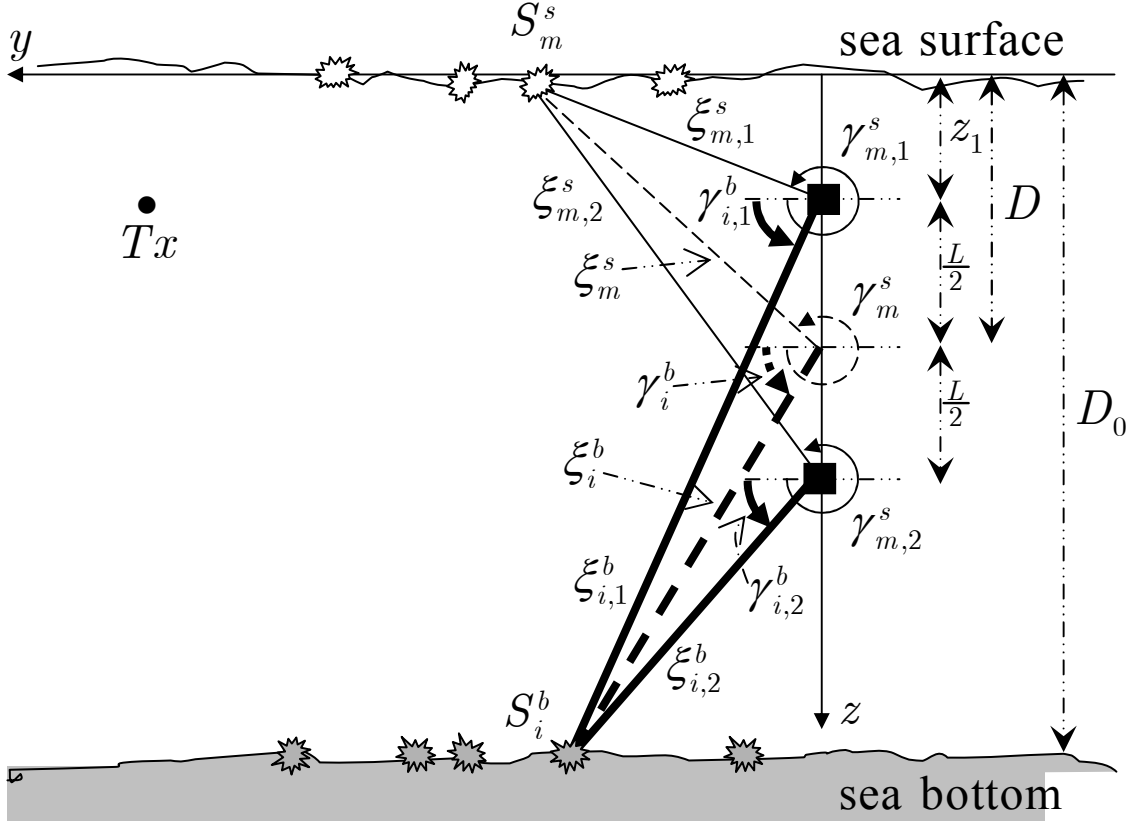


Fig. 2. Geometrical representation of the received rays at the two vector sensors in a shallow water multipath channel.

Let τ and γ represent the delay (travel time) and the AOA (measured with respect to the positive direction of y , counterclockwise). Then in the angle-delay domain, the impulse responses of the pressure subchannels $Tx-Rx_1$ and $Tx-Rx_2$, represented by $\chi_1(\gamma, \tau)$ and $\chi_2(\gamma, \tau)$, respectively, can be written as

$$\begin{aligned} \chi_1(\gamma, \tau) = & (\Lambda_b / N^b)^{1/2} \sum_{i=1}^{N^b} a_i^b \exp(j\psi_i^b) \delta(\gamma - \gamma_{i,1}^b) \delta(\tau - \tau_{i,1}^b) \\ & + ((1 - \Lambda_b) / N^s)^{1/2} \sum_{m=1}^{N^s} a_m^s \exp(j\psi_m^s) \delta(\gamma - \gamma_{m,1}^s) \delta(\tau - \tau_{m,1}^s), \end{aligned} \quad (4)$$

$$\begin{aligned} \chi_2(\gamma, \tau) = & (\Lambda_b / N^b)^{1/2} \sum_{i=1}^{N^b} a_i^b \exp(j\psi_i^b) \delta(\gamma - \gamma_{i,2}^b) \delta(\tau - \tau_{i,2}^b) \\ & + ((1 - \Lambda_b) / N^s)^{1/2} \sum_{m=1}^{N^s} a_m^s \exp(j\psi_m^s) \delta(\gamma - \gamma_{m,2}^s) \delta(\tau - \tau_{m,2}^s). \end{aligned} \quad (5)$$

In eq. (4) and (5), $\delta(\cdot)$ is the Dirac delta, $a_i^b > 0$ and $a_m^s > 0$ represent the amplitudes of the rays scattered from S_i^b and S_m^s , respectively, whereas $\psi_i^b \in [0, 2\pi)$ and $\psi_m^s \in [0, 2\pi)$ stand for the associated phases. The four delay symbols in (4) and (5) represent the travel times from the bottom and surface scatterers to the two vector sensors. For example, $\tau_{i,1}^b$ denotes the travel time from S_i^b to Rx_1 , and so on. As becomes clear in Appendix I, the factors $(N^b)^{-1/2}$ and $(N^s)^{-1/2}$ are included in (4), (5) and the subsequent channel functions, for power normalization. Also $0 \leq \Lambda_b \leq 1$ represents the amount of the contribution of the bottom scatterers, as explained immediately after eq. (51) in Appendix I. A close to one value for Λ_b indicates that most of the received power is coming from the bottom. Of course the amount of the contribution of the surface is given by $1 - \Lambda_b$.

A Dirac delta in the angle domain such as $\delta(\gamma - \tilde{\gamma})$ corresponds to a plane wave with the AOA of $\tilde{\gamma}$, whose equation at an arbitrary point (y, z) is $\exp(jk[y \cos(\tilde{\gamma}) + z \sin(\tilde{\gamma})])$. For example, $\delta(\gamma - \gamma_{i,1}^b)$ in (4) represents $\exp(jk[y \cos(\gamma_{i,1}^b) + z \sin(\gamma_{i,1}^b)])|_{y=0, z=z_1} = \exp(jk z_1 \sin(\gamma_{i,1}^b))$. This is a plane wave emitted from the scatter S_i^b that impinges Rx_1 , located at $y = 0$ and $z = z_1$, through the AOA of $\gamma_{i,1}^b$. Using similar plane wave equations for the other angular delta functions in (4) and (5), the impulse responses of the pressure subchannels $Tx - Rx_1$ and $Tx - Rx_2$ in the delay-space domain can be respectively written as

$$\begin{aligned}
 p_1(\tau) &= (\Lambda_b / N^b)^{1/2} \sum_{i=1}^{N^b} a_i^b \exp(j\psi_i^b) \exp(jk[y \cos(\gamma_{i,1}^b) + z \sin(\gamma_{i,1}^b)]) \delta(\tau - \tau_{i,1}^b) \Big|_{y=0, z=z_1} \\
 &\quad + ((1 - \Lambda_b) / N^s)^{1/2} \sum_{m=1}^{N^s} a_m^s \exp(j\psi_m^s) \exp(jk[y \cos(\gamma_{m,1}^s) + z \sin(\gamma_{m,1}^s)]) \delta(\tau - \tau_{m,1}^s) \Big|_{y=0, z=z_1}, \\
 p_2(\tau) &= (\Lambda_b / N^b)^{1/2} \sum_{i=1}^{N^b} a_i^b \exp(j\psi_i^b) \exp(jk[y \cos(\gamma_{i,2}^b) + z \sin(\gamma_{i,2}^b)]) \delta(\tau - \tau_{i,2}^b) \Big|_{y=0, z=z_1+L} \\
 &\quad + ((1 - \Lambda_b) / N^s)^{1/2} \sum_{m=1}^{N^s} a_m^s \exp(j\psi_m^s) \exp(jk[y \cos(\gamma_{m,2}^s) + z \sin(\gamma_{m,2}^s)]) \delta(\tau - \tau_{m,2}^s) \Big|_{y=0, z=z_1+L}.
 \end{aligned} \tag{6}$$

$$\tag{7}$$

Based on the definition of the spatial Fourier transform [21], $p_1(\tau)$ and $p_2(\tau)$ can be considered as the spatial Fourier transforms of $\chi_1(\gamma, \tau)$ and $\chi_2(\gamma, \tau)$, respectively, with respect to γ . The terms y and z in (6) and (7) are intentionally maintained, as in the sequel we need to calculate the spatial gradients of the pressure with respect to y and z , to obtain the velocities.

By taking the Fourier transform of (6) and (7) with respect to τ , we respectively obtain the complex baseband transfer functions of the pressure subchannels $Tx - Rx_1$ and $Tx - Rx_2$ in the frequency-space domain

$$P_1(f) = (\Lambda_b / N^b)^{1/2} \sum_{i=1}^{N^b} a_i^b \exp(j\psi_i^b) \exp(jk[y \cos(\gamma_{i,1}^b) + z \sin(\gamma_{i,1}^b)]) \exp(-j\omega\tau_{i,1}^b) \Big|_{y=0, z=z_1} \\ + ((1 - \Lambda_b) / N^s)^{1/2} \sum_{m=1}^{N^s} a_m^s \exp(j\psi_m^s) \exp(jk[y \cos(\gamma_{m,1}^s) + z \sin(\gamma_{m,1}^s)]) \exp(-j\omega\tau_{m,1}^s) \Big|_{y=0, z=z_1}, \quad (8)$$

$$P_2(f) = (\Lambda_b / N^b)^{1/2} \sum_{i=1}^{N^b} a_i^b \exp(j\psi_i^b) \exp(jk[y \cos(\gamma_{i,2}^b) + z \sin(\gamma_{i,2}^b)]) \exp(-j\omega\tau_{i,2}^b) \Big|_{y=0, z=z_1+L} \\ + ((1 - \Lambda_b) / N^s)^{1/2} \sum_{m=1}^{N^s} a_m^s \exp(j\psi_m^s) \exp(jk[y \cos(\gamma_{m,2}^s) + z \sin(\gamma_{m,2}^s)]) \exp(-j\omega\tau_{m,2}^s) \Big|_{y=0, z=z_1+L}, \quad (9)$$

where $\omega = 2\pi f$ is used to simplify the notation.

3.2. Velocity-Related Channel Functions

Following the definition of the pressure-equivalent velocity in (2), the velocity channels of interest in the delay-space and frequency-space domains can be written as

$$p_l^y(\tau) = (jk)^{-1} \dot{p}_l(\tau), \quad p_l^z(\tau) = (jk)^{-1} p'_l(\tau), \quad l = 1, 2, \quad (10)$$

$$P_l^y(f) = (jk)^{-1} \dot{P}_l(f), \quad P_l^z(f) = (jk)^{-1} P'_l(f), \quad l = 1, 2, \quad (11)$$

where $p_l(\tau)$ and $P_l(f)$, $l = 1, 2$, are given in (6)-(9). Furthermore, dot and prime denote the partial spatial derivatives $\partial/\partial y$ and $\partial/\partial z$, respectively, of the spatial complex plane waves in (6)-(9). Clearly for $l = 1, 2$, $p_l^y(\tau)$ and $p_l^z(\tau)$ are the pressure-equivalent impulse responses of the velocity subchannels in the y and z directions, respectively. Moreover, $P_l^y(f)$ and $P_l^z(f)$ represent the pressure-equivalent transfer functions of the velocity subchannels in the y and z directions, respectively, with $l = 1, 2$.

4. CORRELATION FUNCTIONS IN VECTOR SENSORS

In a given shallow water channel, obviously the numerical values of all the amplitudes, phases, AOAs and delays in (6)-(9) are complicated functions of environmental characteristics such as the irregular shape of the sea bottom and its layers/losses, volume microstructures, etc. Due to the uncertainty and complexity in exact determination of all these variables, we model

them as random variables. More specifically, we assume all the amplitudes $\{a_i^b\}_i$ and $\{a_m^s\}_m$ are positive uncorrelated random variables, uncorrelated with the phases $\{\psi_i^b\}_i$ and $\{\psi_m^s\}_m$. In addition, all the phases $\{\psi_i^b\}_i$ and $\{\psi_m^s\}_m$ are uncorrelated, uniformly distributed over $[0, 2\pi)$. The statistical properties of the AOAs and delays will be discussed later. Overall, all the pressure and velocity channel functions in (6)-(11) are random processes in space, frequency and delay domains. In what follows, first we derive a closed-form expression for the pressure frequency-space correlation. Then we show how other correlations of interest can be calculated from the pressure frequency-space correlation.

The Pressure Frequency-Space Correlation: We define this correlation as $C_p(\Delta f, L) = E[P_2(f + \Delta f)P_1^*(f)]$, where E and $*$ are mathematical expectation and complex conjugate, respectively. In Appendix I we have derived the following expression

$$C_p(\Delta f, L) = \Lambda_b \int_{\gamma^b=0}^{\pi} w_{\text{bottom}}(\gamma^b) \exp(jk[\varepsilon_y \cos(\gamma^b) + L \sin(\gamma^b)]) \exp(-jT_b \Delta \omega / \sin(\gamma^b)) d\gamma^b \\ + (1 - \Lambda_b) \int_{\gamma^s=\pi}^{2\pi} w_{\text{surface}}(\gamma^s) \exp(jk[\varepsilon_y \cos(\gamma^s) + L \sin(\gamma^s)]) \exp(jT_s \Delta \omega / \sin(\gamma^s)) d\gamma^s, \text{ as } \varepsilon_y \rightarrow 0. \quad (12)$$

In this equation $\Delta \omega = 2\pi \Delta f$ and $\varepsilon_y > 0$ is a small displacement in the y direction, introduced in Appendix I. Moreover, T_b and T_s are defined immediately after (47) in Appendix I. They denote the vertical travel times from the sea bottom to the array center, and from the sea surface to the array center, respectively. Eq. (12) is a frequency-space correlation model for the pressure field which holds for any AOA PDFs with small angle spreads that may be chosen for $w_{\text{bottom}}(\gamma^b)$ and $w_{\text{surface}}(\gamma^s)$. In what follows first we use (12) to derive expressions for various spatial and frequency correlations, which hold for any AOA PDF with small angle spreads. Then in Section 5 we use a flexible parametric PDF for the AOA, to obtain easy-to-use and closed-form expressions for correlations of practical interest.

Now we provide the following two formulas derived from [22], needed in the sequel to calculate velocity-related correlations. Let $\beta(y, z)$ denote a random field in the two-dimensional range-depth plane. Also let $C_\beta(\ell) = E[\beta(y, z + \ell)\beta^*(y, z)]$ be the spatial correlation in the z

direction. Then the correlation functions of the derivative of $\beta(y, z)$ in the z direction, i.e., $\beta'(y, z) = \partial\beta(y, z)/\partial z$ can be written as

$$E[\beta(y, z + \ell)\{\beta'(y, z)\}^*] = -\partial C_\beta(\ell)/\partial \ell, \quad (13)$$

$$E[\beta'(y, z + \ell)\{\beta'(y, z)\}^*] = -\partial^2 C_\beta(\ell)/\partial \ell^2. \quad (14)$$

Similar results hold for the derivative of $\beta(y, z)$ in the y direction, i.e., $\dot{\beta}(y, z) = \partial\beta(y, z)/\partial y$.

4.1. Spatial Correlations for Two Vector Sensors at the Same Frequency

(a) Pressure Correlation: At a fixed frequency with $\Delta f = 0$, the spatial pressure correlation can be obtained from (12) as

$$C_p(0, L) = \int_{\gamma=0}^{2\pi} w(\gamma) \exp(jk[\varepsilon_y \cos(\gamma) + L \sin(\gamma)]) d\gamma, \text{ as } \varepsilon_y \rightarrow 0, \quad (15)$$

where the overall AOA PDF $w(\gamma)$ is defined as follows, to include both the bottom and surface AOAs

$$w(\gamma) = \Lambda_b w_{\text{bottom}}(\gamma) + (1 - \Lambda_b) w_{\text{surface}}(\gamma). \quad (16)$$

Of course $w_{\text{bottom}}(\gamma) = 0$ for $\pi < \gamma < 2\pi$, whereas $w_{\text{surface}}(\gamma) = 0$ for $0 < \gamma < \pi$. We keep (15) as it is, i.e., without replacing ε_y by zero. This is because as we will see in the sequel, we need to take the derivative of $C_p(0, L)$ with respect to ε_y first, then replace ε_y by zero.

(b) Pressure-Velocity Correlations: First we look at the z -component of the velocity. Here we are interested in $E[P_2(f)\{P_1^z(f)\}^*] = (-jk)^{-1} E[P_2(f)\{P_1'(f)\}^*]$, where $P_1^z(f)$ is replaced according to (11). On the other hand, similar to (13), one has $E[P_2(f)\{P_1'(f)\}^*] = -\partial E[P_2(f)P_1^*(f)]/\partial L = -\partial C_p(0, L)/\partial L$. Therefore $E[P_2(f)\{P_1^z(f)\}^*] = (jk)^{-1} \partial C_p(0, L)/\partial L = \int_{\gamma=0}^{2\pi} w(\gamma) \sin(\gamma) \exp(jk[\varepsilon_y \cos(\gamma) + L \sin(\gamma)]) d\gamma, \text{ as } \varepsilon_y \rightarrow 0,$ (17)

where the integral in (17) is coming from (15). An interesting observation can be made when $w(\gamma)$ is even-symmetric with respect to the y axis (symmetry of the AOAs from the bottom and the surface with respect to the horizontal axis y). Then with $L = 0$ in (17) we obtain $E[P_1(f)\{P_1^z(f)\}^*] = 0$, i.e., the co-located pressure and the z -component of the velocity are uncorrelated.

Now we focus on the y -component of the velocity. The correlation of interest is $E[P_2(f)\{P_1^y(f)\}^*] = (-jk)^{-1}E[P_2(f)\{\dot{P}_1(f)\}^*]$, where $P_1^y(f)$ is replaced according to (11). Note that according to the representations for $P_2(f)$ and $P_1(f)$ in (49) and (48), respectively, the location of the second vector sensor can be thought of as $(y, z) = (\varepsilon_y, z_1 + L)$, as $\varepsilon_y \rightarrow 0$, whereas the first vector sensor is located at $(y, z) = (0, z_1)$. So, using the analogous of (13) in the y direction we obtain $E[P_2(f)\{\dot{P}_1(f)\}^*] = -\partial E[P_2(f)P_1^*(f)]/\partial \varepsilon_y$ as $\varepsilon_y \rightarrow 0 = -\partial C_p(0, L)/\partial \varepsilon_y$ as $\varepsilon_y \rightarrow 0$. Differentiation of (15) with respect to ε_y results in

$$\begin{aligned} E[P_2(f)\{P_1^y(f)\}^*] &= (jk)^{-1}\partial C_p(0, L)/\partial \varepsilon_y \text{ as } \varepsilon_y \rightarrow 0, \\ &= \int_{\gamma=0}^{2\pi} w(\gamma)\cos(\gamma)\exp(jk[\varepsilon_y\cos(\gamma) + L\sin(\gamma)])d\gamma, \text{ as } \varepsilon_y \rightarrow 0. \end{aligned} \quad (18)$$

If $w(\gamma)$ is even-symmetric around the z axis, then with $L=0$ in (18) we obtain $E[P_1(f)\{P_1^y(f)\}^*] = 0$, i.e., the co-located pressure and the y -component of the velocity become uncorrelated.

(c) Velocity Correlations: Here we start with the z -component of the velocity. We are going to calculate $E[P_2^z(f)\{P_1^z(f)\}^*] = k^{-2}E[P_2'(f)\{P_1'(f)\}^*]$, where $P_2^z(f)$ and $P_1^z(f)$ are replaced according to (11). On the other hand, similar to (14), one can write $E[P_2'(f)\{P_1'(f)\}^*] = -\partial^2 E[P_2(f)P_1^*(f)]/\partial L^2 = -\partial^2 C_p(0, L)/\partial L^2$. Hence $E[P_2^z(f)\{P_1^z(f)\}^*] = -k^{-2}\partial^2 C_p(0, L)/\partial L^2 = \int_{\gamma=0}^{2\pi} w(\gamma)\sin^2(\gamma)\exp(jk[\varepsilon_y\cos(\gamma) + L\sin(\gamma)])d\gamma$, as $\varepsilon_y \rightarrow 0$,

$$(19)$$

where (15) is used to write the integral in (19).

Let us now concentrate on the y -component of the velocity. In this case the correlation is $E[P_2^y(f)\{P_1^y(f)\}^*] = k^{-2}E[\dot{P}_2(f)\{\dot{P}_1(f)\}^*]$, in which $P_2^y(f)$ and $P_1^y(f)$ are replaced using to (11). As mentioned before (18), the second and the first vector sensors are located at $(y, z) = (\varepsilon_y, z_1 + L)$, as $\varepsilon_y \rightarrow 0$, and $(y, z) = (0, z_1)$, respectively. Thus, by using the equivalent of (14) in the y direction we obtain $E[\dot{P}_2(f)\{\dot{P}_1(f)\}^*] = -\partial^2 E[P_2(f)P_1^*(f)]/\partial \varepsilon_y^2$ as $\varepsilon_y \rightarrow 0 = -\partial^2 C_p(0, L)/\partial \varepsilon_y^2$ as $\varepsilon_y \rightarrow 0$. Taking the second derivative of (15) with respect to ε_y results in

$$\begin{aligned}
E[P_2^y(f)\{P_1^y(f)\}^*] &= -k^{-2}\partial^2 C_p(0,L)/\partial\epsilon_y^2 \text{ as } \epsilon_y \rightarrow 0, \\
&= \int_{\gamma=0}^{2\pi} w(\gamma)\cos^2(\gamma)\exp(jk[\epsilon_y\cos(\gamma)+L\sin(\gamma)])d\gamma, \text{ as } \epsilon_y \rightarrow 0.
\end{aligned} \tag{20}$$

The (average) received powers via the pressure-equivalent velocity channels in the z and y directions are $E[|P_1^z(f)|^2]$ and $E[|P_1^y(f)|^2]$, respectively. Using (19) and (20) with $L = 0$, and since $\sin^2(\gamma) < 1$ and $\cos^2(\gamma) < 1$, one can easily show

$$E[|P_1^z(f)|^2] < 1, \quad E[|P_1^y(f)|^2] < 1, \quad E[|P_1^z(f)|^2] + E[|P_1^y(f)|^2] = 1. \tag{21}$$

Therefore, the received powers via the two velocity channels are not equal. However, through both of them together we receive the same total power that a pressure sensor collects, as shown by the last equation in (21). Note that in this paper the power received by a pressure sensor is $E[|P_1(f)|^2] = C_p(0,0) = 1$, obtained from (15).

Finally, the correlation between the z and y components of the velocity is $E[P_2^z(f)\{P_1^y(f)\}^*] = k^{-2}E[P_2'(f)\{\dot{P}_1(f)\}^*]$, with $P_2^z(f)$ and $P_1^y(f)$ substituted according to (11). A straightforward generalization of (14) results in $E[P_2'(f)\{\dot{P}_1(f)\}^*] = -\partial^2 E[P_2(f)P_1^*(f)]/\partial L\partial\epsilon_y$ as $\epsilon_y \rightarrow 0 = -\partial^2 C_p(0,L)/\partial L\partial\epsilon_y$ as $\epsilon_y \rightarrow 0$. By taking the derivatives of (15) with respect to L and ϵ_y we obtain

$$\begin{aligned}
E[P_2^z(f)\{P_1^y(f)\}^*] &= -k^{-2}\partial^2 C_p(0,L)/\partial L\partial\epsilon_y \text{ as } \epsilon_y \rightarrow 0, \\
&= \int_{\gamma=0}^{2\pi} w(\gamma)\sin(\gamma)\cos(\gamma)\exp(jk[\epsilon_y\cos(\gamma)+L\sin(\gamma)])d\gamma, \text{ as } \epsilon_y \rightarrow 0.
\end{aligned} \tag{22}$$

With $L = 0$, there are two possibilities for which (22) becomes zero: $w(\gamma)$ is even-symmetric with respect to the y axis, or $w(\gamma)$ is even-symmetric around the z axis. In both cases the co-located z and y components of the velocity are uncorrelated.

4.2. Frequency-Space Correlations for Two Vector Sensors

To investigate the frequency-space correlation between the channels of the two vector sensors of Fig. 1, one needs to replace $P_2(f)$ in equations (17)-(20) and (22) of Subsection 4.1 with $P_2(f + \Delta f)$. This provides us with the following equations for the frequency-space correlations between the two vector sensor receivers.

(a) Pressure-Velocity Correlations:

$$E[P_2(f + \Delta f)\{P_1^z(f)\}^*] = (jk)^{-1} \partial C_p(\Delta f, L) / \partial L, \quad (23)$$

$$E[P_2(f + \Delta f)\{P_1^y(f)\}^*] = (jk)^{-1} \partial C_p(\Delta f, L) / \partial \varepsilon_y, \text{ as } \varepsilon_y \rightarrow 0. \quad (24)$$

(b) Velocity Correlations:

$$E[P_2^z(f + \Delta f)\{P_1^z(f)\}^*] = -k^{-2} \partial^2 C_p(\Delta f, L) / \partial L^2, \quad (25)$$

$$E[P_2^y(f + \Delta f)\{P_1^y(f)\}^*] = -k^{-2} \partial^2 C_p(\Delta f, L) / \partial \varepsilon_y^2, \text{ as } \varepsilon_y \rightarrow 0, \quad (26)$$

$$E[P_2^z(f + \Delta f)\{P_1^y(f)\}^*] = -k^{-2} \partial^2 C_p(\Delta f, L) / \partial L \partial \varepsilon_y, \text{ as } \varepsilon_y \rightarrow 0. \quad (27)$$

For any given $C_p(\Delta f, L)$, the above correlations can be easily calculated by taking the derivatives. In what follows, one model for $C_p(\Delta f, L)$ is provided and different types of correlations are calculated.

5. A CASE STUDY

Here we consider the case where the two-element vector sensor array in Fig. 2 receives signal through two beams: one from the bottom with mean AOA μ_b and angle spread σ_b , and the other one from the surface with mean AOA μ_s and angle spread σ_s . When the angle spreads are small, one can model the AOAs with the following Gaussian PDFs

$$\begin{aligned} w_{\text{bottom}}(\gamma^b) &= (2\pi\sigma_b^2)^{-1/2} \exp[-(\gamma^b - \mu_b)^2 / (2\sigma_b^2)], \quad 0 < \gamma^b < \pi, \\ w_{\text{surface}}(\gamma^s) &= (2\pi\sigma_s^2)^{-1/2} \exp[-(\gamma^s - \mu_s)^2 / (2\sigma_s^2)], \quad \pi < \gamma^s < 2\pi. \end{aligned} \quad (28)$$

For large angle spreads, one can use the von Mises PDF [23] [24]. In Fig. 3 these two PDFs are plotted in both linear and polar coordinates.

The first-order Taylor expansion of γ^b around μ_b gives the following results

$$\begin{aligned} \cos(\gamma^b) &\approx \cos(\mu_b) - \sin(\mu_b)(\gamma^b - \mu_b), \\ \sin(\gamma^b) &\approx \sin(\mu_b) + \cos(\mu_b)(\gamma^b - \mu_b), \\ \frac{1}{\sin(\gamma^b)} &\approx \frac{1}{\sin(\mu_b)} - \frac{1}{\sin(\mu_b)} \frac{1}{\tan(\mu_b)} (\gamma^b - \mu_b), \end{aligned} \quad (29)$$

where $\tan(\cdot) = \sin(\cdot) / \cos(\cdot)$. Of course similar relations can be obtained for γ^s . The utility of these first-order expansions comes from the considered small angle spreads, which means the

AOAs γ^b and γ^s are mainly concentrated around μ_b and μ_s , respectively. By substituting these relations into (12), $C_p(\Delta f, L)$ can be written as

$$\begin{aligned}
 C_p(\Delta f, L) &\approx \Lambda_b \exp\left(jk\varepsilon_y \cos(\mu_b) + jkL \sin(\mu_b) - j[\sin(\mu_b)]^{-1} T_b \Delta \omega\right) \\
 &\times \int_{\gamma^b=0}^{\pi} w_{\text{bottom}}(\gamma^b) \exp\left[j\left(-k\varepsilon_y \sin(\mu_b) + kL \cos(\mu_b) + [\sin(\mu_b) \tan(\mu_b)]^{-1} T_b \Delta \omega\right)(\gamma^b - \mu_b)\right] d\gamma^b \\
 &+ (1 - \Lambda_b) \exp\left(jk\varepsilon_y \cos(\mu_s) + jkL \sin(\mu_s) + j[\sin(\mu_s)]^{-1} T_s \Delta \omega\right) \\
 &\times \int_{\gamma^s=\pi}^{2\pi} w_{\text{surface}}(\gamma^s) \exp\left[j\left(-k\varepsilon_y \sin(\mu_s) + kL \cos(\mu_s) - [\sin(\mu_s) \tan(\mu_s)]^{-1} T_s \Delta \omega\right)(\gamma^s - \mu_s)\right] d\gamma^s, \text{ as } \varepsilon_y \rightarrow 0.
 \end{aligned} \tag{30}$$

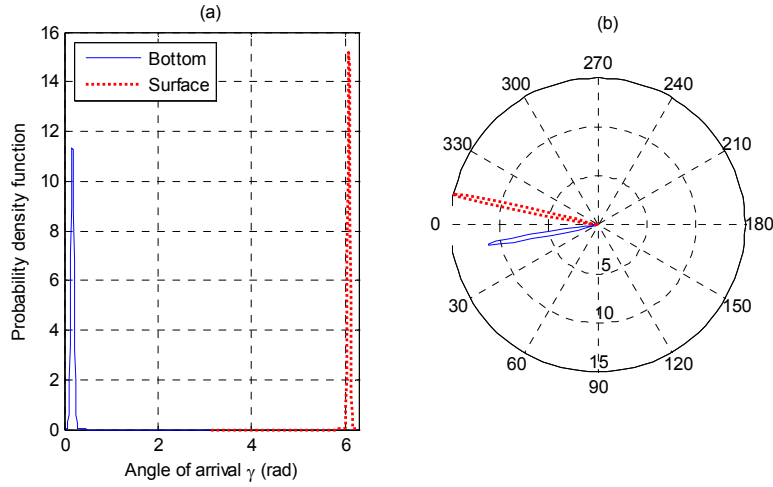


Fig. 3. The bottom and surface angle-of-arrival Gaussian PDFs in (28), with $\sigma_b = \pi/90$ (2°), $\mu_b = \pi/18$ (10°), $\sigma_s = \pi/120$ (1.5°) and $\mu_s = 348\pi/180$ ($348^\circ \equiv -12^\circ$): (a) linear plot, (b) polar plot.

The integrals in (30) resemble the characteristic function of a zero-mean Gaussian variable, which is $\int \exp(j\theta x) (2\pi\sigma^2)^{-1/2} \exp[-x^2/(2\sigma^2)] dx = \exp(-\sigma^2\theta^2/2)$ [22]. This simplifies (30) to the following closed form

$$\begin{aligned}
 C_p(\Delta f, L) &= \Lambda_b \exp\left[j\left(k\varepsilon_y \cos(\mu_b) + kL \sin(\mu_b) - [\sin(\mu_b)]^{-1} T_b \Delta \omega\right)\right] \\
 &\times \exp\left[-0.5\sigma_b^2 \left(-k\varepsilon_y \sin(\mu_b) + kL \cos(\mu_b) + [\sin(\mu_b) \tan(\mu_b)]^{-1} T_b \Delta \omega\right)^2\right] \\
 &+ (1 - \Lambda_b) \exp\left[j\left(k\varepsilon_y \cos(\mu_s) + kL \sin(\mu_s) + [\sin(\mu_s)]^{-1} T_s \Delta \omega\right)\right] \\
 &\times \exp\left[-0.5\sigma_s^2 \left(-k\varepsilon_y \sin(\mu_s) + kL \cos(\mu_s) - [\sin(\mu_s) \tan(\mu_s)]^{-1} T_s \Delta \omega\right)^2\right], \text{ as } \varepsilon_y \rightarrow 0.
 \end{aligned} \tag{31}$$

According to (31) we have $C_p(0,0) = 1$, consistent with the convention of unit (total average) received pressure power, introduced in Appendix I. By taking the derivatives of (31) with respect

to L and ε_y , as listed in (23)-(27), closed-form expressions for a variety of correlations in vector sensor receivers can be obtained. In what follows we focus on spatial correlations for two vector sensors at the same frequency and frequency correlations for a single vector sensor.

5.1. Spatial Correlations for Two Vector Sensors at the Same Frequency

(a) Pressure Correlation: With $\Delta f = 0$, (31) reduces to

$$C_p(0, L) = \Lambda_b \exp[jkL \sin(\mu_b) - 0.5 \sigma_b^2 k^2 L^2 \cos^2(\mu_b)] + (1 - \Lambda_b) \exp[jkL \sin(\mu_s) - 0.5 \sigma_s^2 k^2 L^2 \cos^2(\mu_s)]. \quad (32)$$

The magnitude of (32) is plotted in Fig. 4. To show the accuracy of (32), the exact but more complex equation for the pressure correlation is derived in Appendix II, eq. (61), and is plotted in Fig. 4. The close agreement between the two curves verifies the usefulness of the approximate yet simpler pressure spatial correlation model in (32).

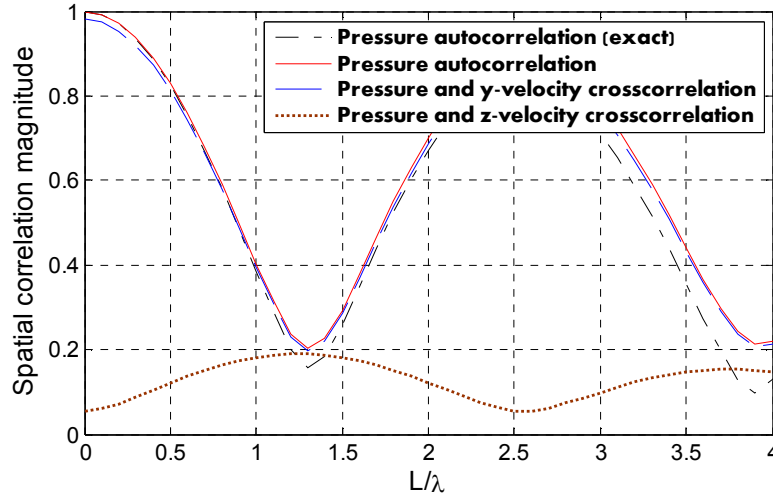


Fig. 4. The magnitudes of the pressure spatial autocorrelation in (32) and pressure-velocity spatial crosscorrelations in (33) and (34) versus L/λ , with $\Lambda_b = 0.4$, $\sigma_b = \pi/90$ (2°), $\mu_b = \pi/18$ (10°), $\sigma_s = \pi/120$ (1.5°), $\mu_s = 348\pi/180$ ($348^\circ \equiv -12^\circ$).

(b) Pressure-Velocity Correlations: By taking the derivative of (32) with respect to L we obtain

$$E[P_2(f)\{P_1^z(f)\}^*] = \Lambda_b[\sin(\mu_b) + j\sigma_b^2 kL \cos^2(\mu_b)] \exp[jkL \sin(\mu_b) - 0.5 \sigma_b^2 k^2 L^2 \cos^2(\mu_b)] + (1 - \Lambda_b)[\sin(\mu_s) + j\sigma_s^2 kL \cos^2(\mu_s)] \exp[jkL \sin(\mu_s) - 0.5 \sigma_s^2 k^2 L^2 \cos^2(\mu_s)]. \quad (33)$$

Moreover, differentiation of (31) with respect to ε_y at $\Delta f = 0$ results in

$$E[P_2(f)\{P_1^y(f)\}^*] = \Lambda_b[\cos(\mu_b) - j\sigma_b^2 kL \sin(\mu_b)\cos(\mu_b)]\exp[jkL \sin(\mu_b) - 0.5\sigma_b^2 k^2 L^2 \cos^2(\mu_b)] \\ + (1 - \Lambda_b)[\cos(\mu_s) - j\sigma_s^2 kL \sin(\mu_s)\cos(\mu_s)]\exp[jkL \sin(\mu_s) - 0.5\sigma_s^2 k^2 L^2 \cos^2(\mu_s)] \quad (34)$$

For $L = 0$, i.e., a single vector sensor, co-located pressure/vertical-velocity and co-located pressure/horizontal-velocity correlations are $\Lambda_b \sin(\mu_b) + (1 - \Lambda_b)\sin(\mu_s)$ and $\Lambda_b \cos(\mu_b) + (1 - \Lambda_b)\cos(\mu_s)$, respectively. As an example, let $\Lambda_b = 0.4$, $\sigma_b = \pi/90$ (2°), $\mu_b = \pi/18$ (10°), $\sigma_s = \pi/120$ (1.5°), and $\mu_s = 348\pi/180$ ($348^\circ \equiv -12^\circ$). This results in -0.055 and 0.98 for P_1/P_1^z and P_1/P_1^y correlations, respectively. Plots of the magnitudes of (33) and (34) are provided in Fig. 4.

(c) Velocity Correlations: By taking the second derivatives of (31) according to (25)-(27) at $\Delta f = 0$ we get

$$E[P_2^z(f)\{P_1^z(f)\}^*] = \Lambda_b[\sin^2(\mu_b) + \sigma_b^2 \cos^2(\mu_b) - \sigma_b^4 k^2 L^2 \cos^4(\mu_b) + j2\sigma_b^2 kL \sin(\mu_b)\cos^2(\mu_b)] \\ \times \exp[jkL \sin(\mu_b) - 0.5\sigma_b^2 k^2 L^2 \cos^2(\mu_b)] \\ + (1 - \Lambda_b)[\sin^2(\mu_s) + \sigma_s^2 \cos^2(\mu_s) - \sigma_s^4 k^2 L^2 \cos^4(\mu_s) + j2\sigma_s^2 kL \sin(\mu_s)\cos^2(\mu_s)] \\ \times \exp[jkL \sin(\mu_s) - 0.5\sigma_s^2 k^2 L^2 \cos^2(\mu_s)], \quad (35)$$

$$E[P_2^y(f)\{P_1^y(f)\}^*] = \Lambda_b[\cos^2(\mu_b) + \sigma_b^2 \sin^2(\mu_b) - \sigma_b^4 k^2 L^2 \sin^2(\mu_b)\cos^2(\mu_b) - j2\sigma_b^2 kL \sin(\mu_b)\cos^2(\mu_b)] \\ \times \exp[jkL \sin(\mu_b) - 0.5\sigma_b^2 k^2 L^2 \cos^2(\mu_b)] \\ + (1 - \Lambda_b)[\cos^2(\mu_s) + \sigma_s^2 \sin^2(\mu_s) - \sigma_s^4 k^2 L^2 \sin^2(\mu_s)\cos^2(\mu_s) - j2\sigma_s^2 kL \sin(\mu_s)\cos^2(\mu_s)] \\ \times \exp[jkL \sin(\mu_s) - 0.5\sigma_s^2 k^2 L^2 \cos^2(\mu_s)], \quad (36)$$

$$E[P_2^z(f)\{P_1^y(f)\}^*] = \\ \Lambda_b[(1 - \sigma_b^2)\sin(\mu_b)\cos(\mu_b) + \sigma_b^4 k^2 L^2 \sin(\mu_b)\cos^3(\mu_b) - jkL\sigma_b^2 \cos(\mu_b)\{\sin^2(\mu_b) - \cos^2(\mu_b)\}] \\ \times \exp[jkL \sin(\mu_b) - 0.5\sigma_b^2 k^2 L^2 \cos^2(\mu_b)] \\ + (1 - \Lambda_b)[(1 - \sigma_s^2)\sin(\mu_s)\cos(\mu_s) + \sigma_s^4 k^2 L^2 \sin(\mu_s)\cos^3(\mu_s) - jkL\sigma_s^2 \cos(\mu_s)\{\sin^2(\mu_s) - \cos^2(\mu_s)\}] \\ \times \exp[jkL \sin(\mu_s) - 0.5\sigma_s^2 k^2 L^2 \cos^2(\mu_s)]. \quad (37)$$

For a single vector sensor, by plugging $L = 0$ into the above equations we obtain

$$E[|P_1^z(f)|^2] = \Lambda_b[\sin^2(\mu_b) + \sigma_b^2 \cos^2(\mu_b)] + (1 - \Lambda_b)[\sin^2(\mu_s) + \sigma_s^2 \cos^2(\mu_s)] \\ \approx \Lambda_b \sin^2(\mu_b) + (1 - \Lambda_b)\sin^2(\mu_s), \quad (38)$$

$$E[|P_1^y(f)|^2] = \Lambda_b[\cos^2(\mu_b) + \sigma_b^2 \sin^2(\mu_b)] + (1 - \Lambda_b)[\cos^2(\mu_s) + \sigma_s^2 \sin^2(\mu_s)] \approx \Lambda_b \cos^2(\mu_b) + (1 - \Lambda_b) \cos^2(\mu_s), \quad (39)$$

$$E[P_1^z(f)\{P_1^y(f)\}^*] = \Lambda_b(1 - \sigma_b^2)\sin(\mu_b)\cos(\mu_b) + (1 - \Lambda_b)(1 - \sigma_s^2)\sin(\mu_s)\cos(\mu_s) \approx (1/2)[\Lambda_b \sin(2\mu_b) + (1 - \Lambda_b)\sin(2\mu_s)]. \quad (40)$$

The almost equal sign \approx in (38)-(40) comes from the assumption of $\sigma_b, \sigma_s \ll 1$ in this case study. As a numerical example, let $\Lambda_b = 0.4$, $\sigma_b = \pi/90$ (2°), $\mu_b = \pi/18$ (10°), $\sigma_s = \pi/120$ (1.5°), and $\mu_s = 348\pi/180$ ($348^\circ \equiv -12^\circ$). According to (38) and (39), the average powers of the vertical and horizontal velocity channels are 0.038 and 0.962, respectively. Furthermore, the correlation between the vertical and horizontal channels is -0.0536 , calculated using (40). Plots of the magnitudes of (35)-(37) are provided in Fig. 5.

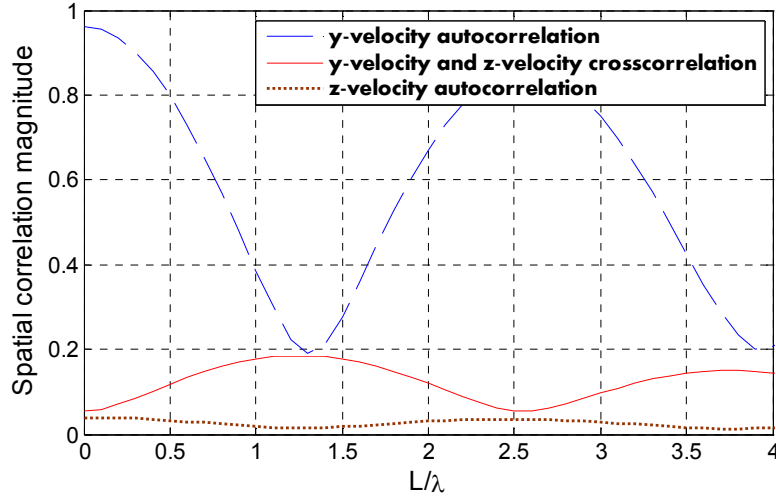


Fig. 5. The magnitudes of the velocity spatial autocorrelations in (35) and (36), and velocity-velocity spatial crosscorrelation in (37) versus L/λ , with $\Lambda_b = 0.4$, $\sigma_b = \pi/90$ (2°), $\mu_b = \pi/18$ (10°), $\sigma_s = \pi/120$ (1.5°), $\mu_s = 348\pi/180$ ($348^\circ \equiv -12^\circ$).

5.2. Frequency Correlations for One Vector Sensor

(a) Pressure Correlation: With $L = 0$ in (31) we obtain

$$\begin{aligned} C_p(\Delta f, 0) &= \Lambda_b \exp(-j[\sin(\mu_b)]^{-1} T_b \Delta \omega) \\ &\quad \times \exp[-0.5 \sigma_b^2 [\sin(\mu_b) \tan(\mu_b)]^{-2} T_b^2 (\Delta \omega)^2] \\ &\quad + (1 - \Lambda_b) \exp(j[\sin(\mu_s)]^{-1} T_s \Delta \omega) \\ &\quad \times \exp[-0.5 \sigma_s^2 [\sin(\mu_s) \tan(\mu_s)]^{-2} T_s^2 (\Delta \omega)^2]. \end{aligned} \quad (41)$$

The magnitude of (41) is plotted in Fig. 6. To show the accuracy of (41), the exact but more complex equation for the frequency correlation is derived in Appendix II, eq. (61), and is plotted

in Fig. 6. The close agreement between the two curves verifies the usefulness of the approximate yet simpler pressure frequency correlation model in (41).

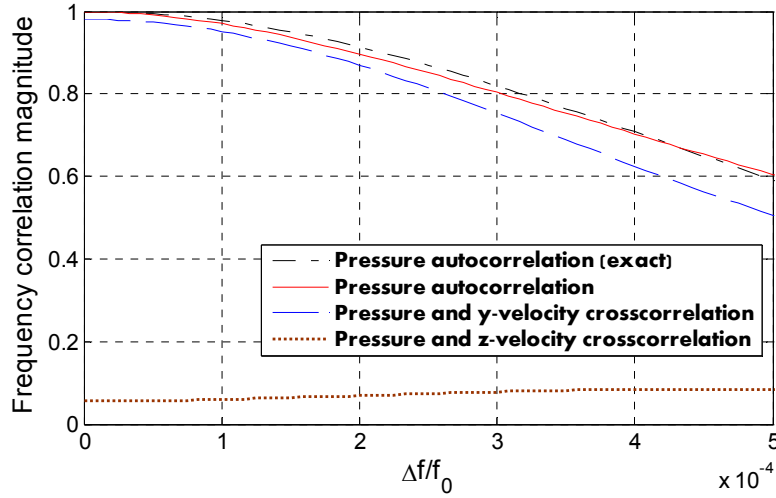


Fig. 6. The magnitudes of the pressure frequency autocorrelation in (41) and the pressure-velocity frequency crosscorrelations in (42) and (43) versus $\Delta f / f_0$, with $f_0 = 12$ kHz, $D_0 = 100$ m, $z_1 = 54$ m, $c = 1500$ m/s, $\Lambda_b = 0.4$, $\sigma_b = \pi / 90$ (2°), $\mu_b = \pi / 18$ (10°), $\sigma_s = \pi / 120$ (1.5°), $\mu_s = 348\pi / 180$ ($348^\circ \equiv -12^\circ$).

(b) Pressure-Velocity Correlations: By applying (23) and (24) to (31) with $L = 0$ one obtains the following results, respectively

$$E[P_1(f + \Delta f)\{P_1^z(f)\}^*] =$$

$$\begin{aligned} & \Lambda_b[\sin(\mu_b) + j\sigma_b^2[\tan(\mu_b)]^{-2}T_b\Delta\omega]\exp[-j[\sin(\mu_b)]^{-1}T_b\Delta\omega - 0.5\sigma_b^2[\sin(\mu_b)\tan(\mu_b)]^{-2}T_b^2(\Delta\omega)^2] \\ & + (1 - \Lambda_b)[\sin(\mu_s) - j\sigma_s^2[\tan(\mu_s)]^{-2}T_s\Delta\omega]\exp[j[\sin(\mu_s)]^{-1}T_s\Delta\omega - 0.5\sigma_s^2[\sin(\mu_s)\tan(\mu_s)]^{-2}T_s^2(\Delta\omega)^2], \end{aligned} \quad (42)$$

$$E[P_1(f + \Delta f)\{P_1^y(f)\}^*] =$$

$$\begin{aligned} & \Lambda_b[\cos(\mu_b) - j\sigma_b^2[\tan(\mu_b)]^{-1}T_b\Delta\omega]\exp[-j[\sin(\mu_b)]^{-1}T_b\Delta\omega - 0.5\sigma_b^2[\sin(\mu_b)\tan(\mu_b)]^{-2}T_b^2(\Delta\omega)^2] \\ & + (1 - \Lambda_b)[\cos(\mu_s) + j\sigma_s^2[\tan(\mu_s)]^{-1}T_s\Delta\omega]\exp[j[\sin(\mu_s)]^{-1}T_s\Delta\omega - 0.5\sigma_s^2[\sin(\mu_s)\tan(\mu_s)]^{-2}T_s^2(\Delta\omega)^2]. \end{aligned} \quad (43)$$

For $\Delta f = 0$, (42) and (43) simplify to the results given in Subsection 5.1. The magnitudes of (42) and (43) are plotted in Fig. 6.

(c) Velocity Correlations: When (25)-(27) are applied to (31), we obtain the following results at $L = 0$, respectively

$$\begin{aligned}
E[P_1^z(f + \Delta f)\{P_1^z(f)\}^*] = & \Lambda_b[\sin^2(\mu_b) + \sigma_b^2 \cos^2(\mu_b) - \sigma_b^4[\tan(\mu_b)]^{-4}T_b^2(\Delta\omega)^2 + j2\sigma_b^2 \cos^2(\mu_b)[\sin(\mu_b)]^{-1}T_b\Delta\omega] \\
& \times \exp[-j[\sin(\mu_b)]^{-1}T_b\Delta\omega - 0.5\sigma_b^2[\sin(\mu_b)\tan(\mu_b)]^{-2}T_b^2(\Delta\omega)^2] \\
& + (1 - \Lambda_b)[\sin^2(\mu_s) + \sigma_s^2 \cos^2(\mu_s) - \sigma_s^4[\tan(\mu_s)]^{-4}T_s^2(\Delta\omega)^2 - j2\sigma_s^2 \cos^2(\mu_s)[\sin(\mu_s)]^{-1}T_s\Delta\omega] \\
& \times \exp[j[\sin(\mu_s)]^{-1}T_s\Delta\omega - 0.5\sigma_s^2[\sin(\mu_s)\tan(\mu_s)]^{-2}T_s^2(\Delta\omega)^2],
\end{aligned} \tag{44}$$

$$\begin{aligned}
E[P_1^y(f + \Delta f)\{P_1^y(f)\}^*] = & \Lambda_b[\cos^2(\mu_b) + \sigma_b^2 \sin^2(\mu_b) - \sigma_b^4[\tan(\mu_b)]^{-2}T_b^2(\Delta\omega)^2 - j2\sigma_b^2 \cos^2(\mu_b)[\sin(\mu_b)]^{-1}T_b\Delta\omega] \\
& \times \exp[-j[\sin(\mu_b)]^{-1}T_b\Delta\omega - 0.5\sigma_b^2[\sin(\mu_b)\tan(\mu_b)]^{-2}T_b^2(\Delta\omega)^2] \\
& + (1 - \Lambda_b)[\cos^2(\mu_s) + \sigma_s^2 \sin^2(\mu_s) - \sigma_s^4[\tan(\mu_s)]^{-2}T_s^2(\Delta\omega)^2 + j2\sigma_s^2 \cos^2(\mu_s)[\sin(\mu_s)]^{-1}T_s\Delta\omega] \\
& \times \exp[j[\sin(\mu_s)]^{-1}T_s\Delta\omega - 0.5\sigma_s^2[\sin(\mu_s)\tan(\mu_s)]^{-2}T_s^2(\Delta\omega)^2],
\end{aligned} \tag{45}$$

$$\begin{aligned}
E[P_1^z(f + \Delta f)\{P_1^y(f)\}^*] = & \Lambda_b[(1 - \sigma_b^2)\sin(\mu_b)\cos(\mu_b) + \sigma_b^4[\tan(\mu_b)]^{-3}T_b^2(\Delta\omega)^2 - j\sigma_b^2[\cos(\mu_b) - \cos^3(\mu_b)[\sin(\mu_b)]^{-1}]T_b\Delta\omega] \\
& \times \exp[-j[\sin(\mu_b)]^{-1}T_b\Delta\omega - 0.5\sigma_b^2[\sin(\mu_b)\tan(\mu_b)]^{-2}T_b^2(\Delta\omega)^2] \\
& + (1 - \Lambda_b)[(1 - \sigma_s^2)\sin(\mu_s)\cos(\mu_s) + \sigma_s^4[\tan(\mu_s)]^{-3}T_s^2(\Delta\omega)^2 + j\sigma_s^2[\cos(\mu_s) - \cos^3(\mu_s)[\sin(\mu_s)]^{-1}]T_s\Delta\omega] \\
& \times \exp[j[\sin(\mu_s)]^{-1}T_s\Delta\omega - 0.5\sigma_s^2[\sin(\mu_s)\tan(\mu_s)]^{-2}T_s^2(\Delta\omega)^2].
\end{aligned} \tag{46}$$

When $\Delta f = 0$, (44)-(46) reduce to (38)-(40). The plots of the magnitudes of (44)-(46) are given in Fig. 7.

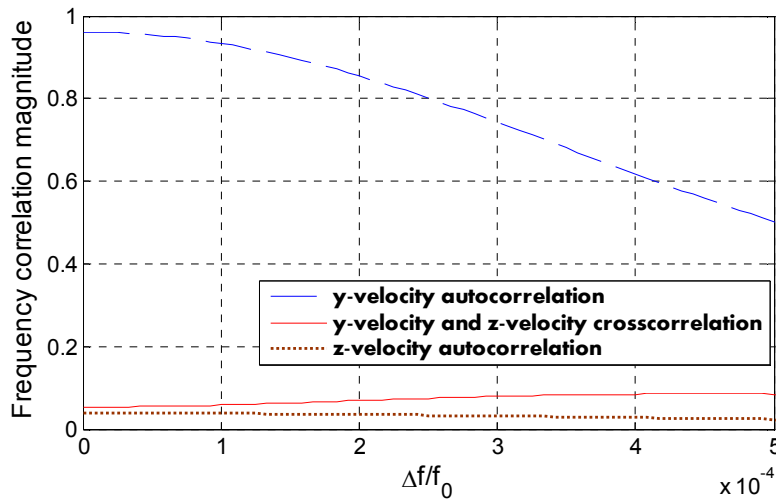


Fig. 7. The magnitudes of the velocity frequency autocorrelations in (44) and (45), and velocity-velocity frequency crosscorrelation in (46) versus $\Delta f / f_0$, with $f_0 = 12$ kHz, $D_0 = 100$ m, $z_1 = 54$ m, $c = 1500$ m/s, $\Lambda_b = 0.4$, $\sigma_b = \pi / 90$ (2°), $\mu_b = \pi / 18$ (10°), $\sigma_s = \pi / 120$ (1.5°), $\mu_s = 348\pi / 180$ ($348^\circ \equiv -12^\circ$).

In the ambient noise field, correlations among the elements of a vector sensor array are calculated in [25]. The emphasis of this manuscript, however, is the development of a geometrical-statistical model for the shallow water waveguide, as shown in Fig. 2 and analyzed in appendices. Upon using Gaussian PDFs for surface- and bottom-reflected AOA, a closed-form integral-free expression is derived in (31) for the pressure field correlation in space and frequency. Another focal point of the present paper is the emphasis on the frequency domain representation of the acoustic field, e.g., the frequency transfer functions in (8) and (9). This allows to derive frequency domain correlations that are important for communication system design. For example, eq. (41) can be used to determine the correlation between two Δf -separated tones received by a vector sensor, in a multi-carrier system such as OFDM (orthogonal frequency division multiplexing). Overall, the proposed shallow water geometrical-statistical channel model provides useful expressions for space-frequency vector sensor correlations, in terms of the physical parameters of the channel such as mean angle of arrivals and angle spreads.

6. COMPARISON WITH MEASURED DATA

To experimentally verify the proposed model, in this section we compare the derived pressure correlation function in (32) with the measured data of [26]. Once the accuracy of the pressure correlation function is experimentally confirmed, one can take the derivatives of the pressure correlation, to find different types of correlations in a vector sensor array, as discussed in previous sections.

A uniform 33-element array with 0.5 m element spacing was deployed at a 10 km range, where the bottom depth was 103 m [26]. The measurements were conducted at the center frequency of $f_0 = 1.2$ kHz. The empirical vertical correlation of the pressure field, estimated from the measured data, is shown in Fig. 8. The vertical correlation in [26] is measured with respect to the eighth element from the bottom of the 33-element array. This explains the horizontal axis in Fig. 8 and the peak value at the eight element. To compare the proposed correlation model in (32) with measured correlation, its parameters need to be determined. We chose $\mu_b = 3^\circ$ and $\mu_s = 353^\circ \equiv -7^\circ$, as according to [26], there are two dominant arrivals from

these directions. After inserting these numbers into (32), the remaining parameters were estimated using a numerical least squares approach. Similarly to [26], the model was compared with the measured correlation over the eight neighboring receivers (elements one to fifteen in Fig. 8). This resulted in $\Lambda_b = 0.56$, $\sigma_b = 0.04$ and $\sigma_s = 0.14$ rad. The magnitude of the proposed model in (32) is plotted in Fig. 8. The close agreement between the model and measured correlations in Fig. 8 indicates the usefulness of the model. As a reference, the exponential model of [26], i.e., $\exp(-L^2/(2\lambda)^2)$ is also included in Fig. 8. Here $\lambda = 1.2$ m is the wavelength. One can observe the proposed model provides a closer match to experimental correlation at the first and fifteenth elements. The main advantage of the proposed model is that it expresses the acoustic field correlation as a function of important physical parameters of the channel such as angle of arrivals and angle spreads. This allows system engineers to understand how these channel parameters affect the correlation, which in turn provides useful guidelines for proper array and system design.

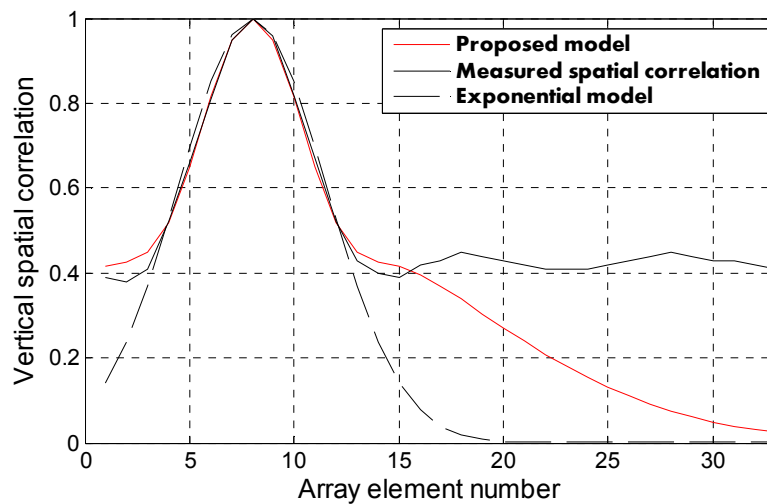


Fig. 8. Comparison of the proposed model with measured data.

7. CONCLUSION

In this paper we have developed a statistical framework for mathematical characterization of different types of correlations in acoustic vector sensor arrays. Closed-form expressions are derived which relate signal correlations to some key channel parameters such as mean angle of arrivals and angle spreads. Using these expressions one can calculate the correlations between

the pressure and velocity channels of the sensors, in terms of element spacing and frequency separation. The results of this paper are useful for the design and performance analysis of vector sensor systems and array processing algorithms.

ACKNOWLEDGEMENT

We would like to thank Dr. T. C. Yang from the Naval Research Laboratory, Washington, DC, for useful discussions regarding experimental data and the underwater spatial correlation.

Appendix I.

A CLOSED-FORM FREQUENCY-SPACE CORRELATION MODEL FOR THE PRESSURE CHANNEL

When angle spreads are small and $L \ll \min(z_1, D_0 - z_1)$, one can approximate the AOAs in (8) and (9) as $\gamma_{i,1}^b \approx \gamma_{i,2}^b \approx \gamma_i^b$ and $\gamma_{m,1}^s \approx \gamma_{m,2}^s \approx \gamma_m^s$, where γ_i^b and γ_m^s are shown in Fig. 2. Furthermore, the traveled distances can be approximated as $\xi_{i,1}^b \approx \xi_{i,2}^b \approx \xi_i^b$ and $\xi_{m,1}^s \approx \xi_{m,2}^s \approx \xi_m^s$, with ξ_i^b and ξ_m^s depicted in Fig. 2. Note that each delay is the traveled distance divided by the sound speed c . Therefore all the delays in (8) and (9) can be approximated by $\tau_{i,1}^b \approx \tau_{i,2}^b \approx \tau_i^b$ and $\tau_{m,1}^s \approx \tau_{m,2}^s \approx \tau_m^s$, where $\tau_i^b = \xi_i^b / c$ and $\tau_m^s = \xi_m^s / c$. According to Fig. 2 it is easy to verify that $\sin(\gamma_i^b) = (D_0 - D) / \xi_i^b$ and $-\sin(\gamma_m^s) = D / \xi_m^s$. Hence

$$\begin{aligned} \tau_i^b &= T_b / \sin(\gamma_i^b), \quad 0 < \gamma_i^b < \pi, \\ \tau_m^s &= -T_s / \sin(\gamma_m^s), \quad \pi < \gamma_m^s < 2\pi. \end{aligned} \quad (47)$$

The parameters $T_b = (D_0 - D) / c$ and $T_s = D / c$ in (47) denote the vertical travel times from the sea bottom to the array center, and from the sea surface to the array center, respectively. Clearly the range of γ_m^s in (47) implies that $-1 \leq \sin(\gamma_m^s) < 0$, which makes τ_m^s non-negative, as expected. In general we have $T_b \leq \tau_i^b < \infty, \forall i$, and $T_s \leq \tau_m^s < \infty, \forall m$. Now (8) and (9) can be simplified as follows

$$\begin{aligned} P_1(f) &= (\Lambda_b / N^b)^{1/2} \sum_{i=1}^{N^b} a_i^b \exp(j\psi_i^b) \exp(jk z_1 \sin(\gamma_i^b)) \exp(-jT_b \omega / \sin(\gamma_i^b)) \\ &\quad + ((1 - \Lambda_b) / N^s)^{1/2} \sum_{m=1}^{N^s} a_m^s \exp(j\psi_m^s) \exp(jk z_1 \sin(\gamma_m^s)) \exp(jT_s \omega / \sin(\gamma_m^s)), \\ P_2(f) &= (\Lambda_b / N^b)^{1/2} \sum_{i=1}^{N^b} a_i^b \exp(j\psi_i^b) \exp(jk [\varepsilon_y \cos(\gamma_i^b) + (z_1 + L) \sin(\gamma_i^b)]) \exp(-jT_b \omega / \sin(\gamma_i^b)) \\ &\quad + ((1 - \Lambda_b) / N^s)^{1/2} \sum_{m=1}^{N^s} a_m^s \exp(j\psi_m^s) \exp(jk [\varepsilon_y \cos(\gamma_m^s) + (z_1 + L) \sin(\gamma_m^s)]) \exp(jT_s \omega / \sin(\gamma_m^s)), \text{ as } \varepsilon_y \rightarrow 0, \end{aligned} \quad (48)$$

$$(49)$$

where $\varepsilon_y > 0$ is a displacement in the y direction. Note that ε_y is introduced to represent the location of the second sensor in Fig. 2 as $(y, z) = (\varepsilon_y, z_1 + L)$, as $\varepsilon_y \rightarrow 0$. This allows to calculate those correlation functions which are related to the horizontal component of the velocity, as discussed in Section 4.

Due to the uniform distribution of all the phases $\{\psi_i^b\}_i$ and $\{\psi_m^s\}_m$ over $[0, 2\pi)$ we have $E[\exp(\pm j\psi_i^b)] = E[\exp(\pm j\psi_m^s)] = 0, \forall i, m$. This results in $E[\exp(\pm j\psi_i^b)\exp(\pm j\psi_m^s)] = 0, \forall i, m$, because all the phases are independent. Similarly we have $E[\exp(j\psi_i^b)\exp(-j\psi_{\tilde{i}}^b)] = 0, \forall i \neq \tilde{i}$ and $E[\exp(j\psi_m^s)\exp(-j\psi_{\tilde{m}}^s)] = 0, \forall m \neq \tilde{m}$. Clearly the last two expressions become 1, when $i = \tilde{i}$ and $m = \tilde{m}$. Therefore, after substituting (48) and (49) into $C_p(\Delta f, L) = E[P_2(f + \Delta f)P_1^*(f)]$, only the following two single summations remain

$$C_p(\Delta f, L) = (\Lambda_b / N^b) \sum_{i=1}^{N^b} E[(a_i^b)^2] \exp(jk[\varepsilon_y \cos(\gamma_i^b) + L \sin(\gamma_i^b)]) \exp(-jT_b \Delta \omega / \sin(\gamma_i^b))$$

$$+ ((1 - \Lambda_b) / N^s) \sum_{m=1}^{N^s} E[(a_m^s)^2] \exp(jk[\varepsilon_y \cos(\gamma_m^s) + L \sin(\gamma_m^s)]) \exp(jT_s \Delta \omega / \sin(\gamma_m^s)), \text{ as } \varepsilon_y \rightarrow 0,$$

(50)

where $\Delta \omega = 2\pi \Delta f$.

The terms $E[(a_i^b)^2] / N^b$ and $E[(a_m^s)^2] / N^s$ in (50) represent the normalized (average) powers received from the two scatterers S_i^b and S_m^s on the sea bottom and its surface, respectively. Let $\sum_{i=1}^{N^b} E[(a_i^b)^2] / N^b = 1$ and $\sum_{m=1}^{N^s} E[(a_m^s)^2] / N^s = 1$. We also define $w_{\text{bottom}}(\gamma^b)$ and $w_{\text{surface}}(\gamma^s)$ as the probability density functions (PDFs) of the AOAs of the waves coming from the sea bottom and its surface, respectively, such that $0 < \gamma^b < \pi$ and $\pi < \gamma^s < 2\pi$. When N^b and N^s are large, one can think of $E[(a_i^b)^2] / N^b$ and $E[(a_m^s)^2] / N^s$ as the normalized powers received through the infinitesimal angles $d\gamma^b$ and $d\gamma^s$, respectively, centered at the AOAs γ_i^b and γ_m^s . Thus, with the chosen normalizations $\sum_{i=1}^{N^b} E[(a_i^b)^2] / N^b = 1$ and $\sum_{m=1}^{N^s} E[(a_m^s)^2] / N^s = 1$, we can write $E[(a_i^b)^2] / N^b = w_{\text{bottom}}(\gamma_i^b) d\gamma^b$ and $E[(a_m^s)^2] / N^s = w_{\text{surface}}(\gamma_m^s) d\gamma^s$. These relations allow the summations in (50) to be replaced by integrals

$$C_p(\Delta f, L) = \Lambda_b \int_{\gamma^b=0}^{\pi} w_{\text{bottom}}(\gamma^b) \exp(jk[\varepsilon_y \cos(\gamma^b) + L \sin(\gamma^b)]) \exp(-jT_b \Delta \omega / \sin(\gamma^b)) d\gamma^b \\ + (1 - \Lambda_b) \int_{\gamma^s=\pi}^{2\pi} w_{\text{surface}}(\gamma^s) \exp(jk[\varepsilon_y \cos(\gamma^s) + L \sin(\gamma^s)]) \exp(jT_s \Delta \omega / \sin(\gamma^s)) d\gamma^s, \text{ as } \varepsilon_y \rightarrow 0. \quad (51)$$

Note that according to (51) we have $C_p(0, 0) = \Lambda_b + (1 - \Lambda_b) = 1$, which represents the convenient unit (total average) received pressure power. The factor $0 \leq \Lambda_b \leq 1$ was defined to stand for the amount of the power coming from the sea bottom, whereas $1 - \Lambda_b$ shows the power coming from the surface.

Appendix II.

THE EXACT FREQUENCY-SPACE CORRELATION OF THE PRESSURE CHANNEL

Here we derive the exact frequency-space correlation of the pressure channel, for the vertical array in the shallow water channel of Fig. 2. By inserting $P_1(f)$ and $P_2(f)$ from (8) and (9) into $C_p(\Delta f, L) = E[P_2(f + \Delta f)P_1^*(f)]$ and upon using the properties of the phases $\{\psi_i^b\}_i$ and $\{\psi_m^s\}_m$, as done in Appendix I, one can show that

$$C_p(\Delta f, L) = (\Lambda_b / N^b) \sum_{i=1}^{N^b} E[(a_i^b)^2] \exp(jkz_1[\sin(\gamma_{i,2}^b) - \sin(\gamma_{i,1}^b)]) \exp(jkL \sin(\gamma_{i,2}^b)) \\ \times \exp(-j\Delta \omega \tau_{i,2}^b) \exp(j\omega(\tau_{i,1}^b - \tau_{i,2}^b)) \\ + ((1 - \Lambda_b) / N^s) \sum_{m=1}^{N^s} E[(a_m^s)^2] \exp(jkz_1[\sin(\gamma_{m,2}^s) - \sin(\gamma_{m,1}^s)]) \exp(jkL \sin(\gamma_{m,2}^s)) \\ \times \exp(-j\Delta \omega \tau_{m,2}^s) \exp(j\omega(\tau_{m,1}^s - \tau_{m,2}^s)). \quad (52)$$

By using the law of cosines in appropriate triangles in Fig. 2, one can obtain the following relations, which are needed for calculating (52), numerically

$$\sin(\gamma_{i,1}^b) = \frac{(D_0 - z_1) \sin(\gamma_i^b)}{\sqrt{(D_0 - z_1 - (L/2))^2 + L(D_0 - z_1 - (L/4)) \sin^2(\gamma_i^b)}}, \quad (53)$$

$$\sin(\gamma_{i,2}^b) = \frac{(D_0 - z_1 - L) \sin(\gamma_i^b)}{\sqrt{(D_0 - z_1 - (L/2))^2 - L(D_0 - z_1 - (3L/4)) \sin^2(\gamma_i^b)}}, \quad (54)$$

$$\tau_{i,1}^b = \frac{\xi_{i,1}^b}{c} = \frac{\sqrt{(D_0 - z_1 - (L/2))^2 + L(D_0 - z_1 - (L/4)) \sin^2(\gamma_i^b)}}{c \sin(\gamma_i^b)}, \quad (55)$$

$$\tau_{i,2}^b = \frac{\xi_{i,2}^b}{c} = \frac{\sqrt{(D_0 - z_1 - (L/2))^2 - L(D_0 - z_1 - (3L/4)) \sin^2(\gamma_i^b)}}{c \sin(\gamma_i^b)}, \quad (56)$$

$$\sin(\gamma_{m,1}^s) = \frac{z_1 \sin(\gamma_m^s)}{\sqrt{(z_1 + (L/2))^2 - L(z_1 + (L/4)) \sin^2(\gamma_m^s)}}, \quad (57)$$

$$\sin(\gamma_{m,2}^s) = \frac{(z_1 + L) \sin(\gamma_m^s)}{\sqrt{(z_1 + (L/2))^2 + L(z_1 + (3L/4)) \sin^2(\gamma_m^s)}}, \quad (58)$$

$$\tau_{m,1}^s = \frac{\xi_{m,1}^s}{c} = \frac{-\sqrt{(z_1 + (L/2))^2 - L(z_1 + (L/4)) \sin^2(\gamma_m^s)}}{c \sin(\gamma_m^s)}, \quad (59)$$

$$\tau_{m,2}^s = \frac{\xi_{m,2}^s}{c} = \frac{-\sqrt{(z_1 + (L/2))^2 + L(z_1 + (3L/4)) \sin^2(\gamma_m^s)}}{c \sin(\gamma_m^s)}. \quad (60)$$

All the \sin 's and τ 's in (53)-(60) are functions of the bottom and surface AOAs γ_i^b and γ_m^s , respectively. As done in Appendix I, when N^b and N^s are large, one can introduce the AOA PDFs as $E[(a_i^b)^2]/N^b = w_{\text{bottom}}(\gamma_i^b)d\gamma^b$ and $E[(a_m^s)^2]/N^s = w_{\text{surface}}(\gamma_m^s)d\gamma^s$. This way the two summations in (52) can be replaced by integrals over γ^b and γ^s , respectively

$$\begin{aligned} C_p(\Delta f, L) = & \Lambda_b \int_{\gamma^b=0}^{\pi} w_{\text{bottom}}(\gamma^b) \exp(jkz_1[\sin(\gamma_2^b) - \sin(\gamma_1^b)]) \exp(jkL \sin(\gamma_2^b)) \\ & \times \exp(-j\Delta\omega\tau_2^b) \exp(j\omega(\tau_1^b - \tau_2^b)) d\gamma^b \\ & + (1 - \Lambda_b) \int_{\gamma^s=\pi}^{2\pi} w_{\text{surface}}(\gamma^s) \exp(jkz_1[\sin(\gamma_2^s) - \sin(\gamma_1^s)]) \exp(jkL \sin(\gamma_2^s)) \\ & \times \exp(-j\Delta\omega\tau_2^s) \exp(j\omega(\tau_1^s - \tau_2^s)) d\gamma^s. \end{aligned} \quad (61)$$

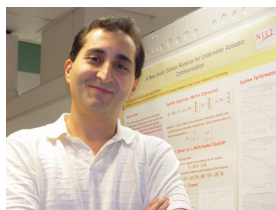
Note that all the \sin 's and τ 's in (61) are exactly the same as those given in (53)-(60), with the subscripts i and m removed.

REFERENCES

- [1] A. Nehorai and E. Paldi, "Acoustic vector-sensor array processing," *IEEE Trans. Signal Processing*, vol. 42, pp. 2481-2491, 1994.
- [2] B. Hochwald and A. Nehorai, "Identifiability in array processing models with vector-sensor applications," *IEEE Trans. Signal Processing*, vol. 44, pp. 83-95, 1996.
- [3] M. D. Zoltowski and K. T. Wong, "Closed-form eigenstructure-based direction finding using arbitrary but identical subarrays on a sparse uniform Cartesian array grid," *IEEE Trans. Signal Processing*, vol. 48, pp. 2205-2210, 2000.
- [4] M. Hawkes and A. Nehorai, "Wideband source localization using a distributed acoustic vector-sensor array," *IEEE Trans. Signal Processing*, vol. 51, pp. 1479-1491, 2003.
- [5] *Proc. AIP Conf. Acoustic Particle Velocity Sensors: Design, Performance, and Applications*, Mystic, CT, 1995.

- [6] *Proc. Workshop Directional Acoustic Sensors (CD-ROM)*, New Port, RI, 2001.
- [7] M. Hawkes and A. Nehorai, "Acoustic vector-sensor beamforming and Capon direction estimation," *IEEE Trans. Signal Processing*, vol. 46, pp. 2291-2304, 1998.
- [8] B. A. Cray and A. H. Nuttall, "Directivity factors for linear arrays of velocity sensors," *J. Acoust. Soc. Am.*, vol. 110, pp. 324-331, 2001.
- [9] A. Abdi and H. Guo, "A new compact multichannel receiver for underwater wireless communication networks," accepted for publication in *IEEE Trans. Wireless Commun.*, 2008.
- [10] A. Abdi, H. Guo and P. Sutthiwan, "A new vector sensor receiver for underwater acoustic communication," in *Proc. MTS/IEEE Oceans*, Vancouver, BC, Canada, 2007.
- [11] T. B. Gabrielson, "Design problems and limitations in vector sensors," in *Proc. Workshop Directional Acoustic Sensors (CD-ROM)*, New Port, RI, 2001.
- [12] M. O. Damen, A. Abdi, and M. Kaveh, "On the effect of correlated fading on several space-time coding and detection schemes," in *Proc. IEEE Vehic. Technol. Conf.*, Atlantic City, NJ, 2001, pp. 13-16.
- [13] M. Chiani, M. Z. Win and A. Zanella, "On the capacity of spatially correlated MIMO Rayleigh-fading channels," *IEEE Trans. Inform. Theory*, vol. 49, pp. 2363-2371, 2003.
- [14] V. K. Nguyen and L. B. White, "Joint space-time trellis decoding and channel estimation in correlated fading channels," *IEEE Signal Processing Lett.*, vol. 11, pp. 633-636, 2004.
- [15] C. B. Ribeiro, E. Ollila and V. Koivunen, "Stochastic maximum-likelihood method for MIMO propagation parameter estimation," *IEEE Trans. Signal Processing*, vol. 55, pp. 46-55, 2007.
- [16] C. B. Ribeiro, A. Richter and V. Koivunen, "Joint angular- and delay-domain MIMO propagation parameter estimation using approximate ML method," *IEEE Trans. Signal Processing*, vol. 55, pp. 4775-4790, 2007.
- [17] A. Abdi and M. Kaveh, "Parametric modeling and estimation of the spatial characteristics of a source with local scattering," in *Proc. IEEE Int. Conf. Acoust., Speech, Signal Processing*, Orlando, FL, 2002, pp. 2821-2824.
- [18] B. A. Cray, V. M. Evora, and A. H. Nuttall, "Highly directional acoustic receivers," *J. Acoust. Soc. Am.*, vol. 113, pp. 1526-1532, 2003.

- [19] A. D. Pierce, *Acoustics: An Introduction to Its Physical Principles and Applications*, 2nd ed., Acoustic Soc. Am., 1989.
- [20] P. C. Etter, *Underwater Acoustic Modeling and Simulation*, 3rd ed., New York: Spon, 2003.
- [21] H. L. Van Trees, *Optimum Array Processing*. New York: Wiley, 2002.
- [22] A. Papoulis, *Probability, Random Variables, and Stochastic Processes*, 3rd ed., Singapore: McGraw-Hill, 1991.
- [23] A. Abdi, J. A. Barger, and M. Kaveh, "A parametric model for the distribution of the angle of arrival and the associated correlation function and power spectrum at the mobile station," *IEEE Trans. Vehic. Technol.*, vol. 51, pp. 425-434, 2002.
- [24] A. Abdi and M. Kaveh, "A space-time correlation model for multielement antenna systems in mobile fading channels," *IEEE J. Select. Areas Commun.*, vol. 20, pp. 550-560, 2002.
- [25] M. Hawkes and A. Nehorai, "Acoustic vector-sensor correlations in ambient noise," *IEEE J. Oceanic Eng.*, vol. 26, pp. 337-347, 2001.
- [26] T. C. Yang, "A study of spatial processing gain in underwater acoustic communications," *IEEE J. Oceanic Eng.*, vol. 32, pp. 689-709, 2007.



Ali Abdi (S'98, M'01, SM'06) received the Ph.D. degree in electrical engineering from the University of Minnesota, Minneapolis, in 2001. He joined the Department of Electrical and Computer Engineering of New Jersey Institute of Technology (NJIT), Newark, in 2001, where he is

currently an Associate Professor. His current research interests include characterization and estimation of wireless channels, digital communication in underwater and terrestrial channels, blind modulation recognition, systems biology and molecular networks. Dr. Abdi was an Associate Editor for IEEE Transactions on Vehicular Technology from 2002 to 2007. He was also the co-chair of the Communication and Information Theory Track of the 2008 IEEE ICCCN (International Conference on Computer Communications and Networks). Dr. Abdi has received 2006 NJIT Excellence in Teaching Award, in the category of Excellence in Team,

Interdepartmental, Multidisciplinary, or Non-Traditional Teaching. He has also received 2008 New Jersey Inventors Hall of Fame (NJIHof) Innovators Award on Acoustic Communication, for his work on underwater acoustic communication.



Huaihai Guo received the master degree in electrical engineering from Cleveland State University. Now he is the Ph.D. candidate in Electrical and Computer Engineering of New Jersey Institute of Technology (NJIT). His current research interests include digital communication in underwater channels via vector sensors, precoding/equalization for acoustic particle velocity channels and multiuser and multiple access system via vector sensors. He is a Student Member of IEEE.